

# On The Effect of Antenna Height On the Characterization of The Indoor UWB Channel

Umesh K. Shukla, Haris I. Volos, and R. Michael Buehrer

Wireless@Virginia Tech

Blacksburg, VA 24061, USA

Email: {ushukla, hvolos, buehrer}@vt.edu

**Abstract**—Ultra-wideband (UWB) technology is being proposed for several short range wireless applications. Some of the applications, such as position location devices for rescue personnel, may require the antenna height to be close to the ground. In scenarios where the antenna height is very low (from 0 to 30 cm), propagation characteristics and channel modeling are needed to provide important insights for the application design. This paper presents time-domain measurements and channel characterization of the indoor UWB channel at three different antenna heights (7.5 cm, 26.5 cm, and 108.5 cm). The transmitting and receiving antennas are placed at heights referred to as near ground, middle ground, and above ground. The effects of the antenna height on the channel characteristics are analyzed. Both large and small-scale characteristics are evaluated and the results for different antenna heights are compared. The results show that large scale characteristics exhibit monotonic behavior with respect to antenna height while small scale characteristics do not follow this behavior. The possible explanations for the obtained results are also discussed.

## I. INTRODUCTION

Ultra-wideband (UWB) has emerged as a promising technology for a range of communication applications. It has been proposed for use in applications such as position location devices for rescue personnel, wireless personal area networks, and security systems [1]. In addition, many applications like border patrol and homeland security require sensor networks to be positioned on the ground [2]. Finally, there are also possible scenarios in military applications that require low antenna height (less than 50 cm) [3]. These applications can also be used in indoor scenarios. This provides a motivation for characterizing the indoor near-ground UWB channel. We call a channel ‘near-ground’ when the heights of transmit (Tx) and receive (Rx) antennas are under 10 cm.

The characterization of a channel requires the availability of sample measurement data in various environments. In the recent years significant amounts of data have been gathered [4], [5], [6], [7] to investigate the effects of different environments on UWB propagation. However, with the exception of our previous work presented in [8], few results exist on the effects of placing the antennas on the ground. There are few studies on near ground propagation ([9], [3], [10]) but either they do not consider UWB systems or consider the outdoor scenario. Although [8] provides a characterization of the near-ground channel, there are few remaining issues. First, it only considers two heights: 7.5 cm and 108.5 cm; It does not consider an intermediate case such as 30 cm which could

be an important application as described in [3]. As it will be shown, not all the channel characteristics for this height can be directly inferred from the characteristics of the other two heights. Second, [8] lacks in providing explanations for the obtained results, especially for the small scale characteristics (SSC).

The contribution of this paper is to complement [8] by addressing the issues mentioned above. The use of three different antenna heights allows us to reach stronger conclusions about the effect of the height on the channel characteristics. Furthermore, the paper focuses more on the SSC, which are very important for receiver design. In addition, it examines the variation of the Root Mean Square (RMS) delay spread for 13 different heights between 7.5 cm and 135 cm. Possible explanations for the results are also provided.

The rest of the paper is organized as follows: First, section II provides a description of the measurement setup. Second, section III discusses the analysis performed. Third, section IV presents and discusses the results from the analysis. Finally, section V ends the paper with some concluding remarks.

## II. MEASUREMENT SETUP

### A. Measurement system

The experiments were conducted by transmitting an unmodulated baseband pulse using the Geozondas GZ1106DL1 and GZ1117DN-25 main unit and pulsing head respectively which produces a Gaussian like pulse with 30 V peak at 50  $\Omega$  and half amplitude width of 30 ps. The generated pulse was applied to a bicone antenna. A digital oscilloscope was used to receive the signal from an identical bicone antenna with a 12.5 ps sampling resolution over a 50 ns window (it was observed that very little multipath energy existed beyond an excess delay of 50 ns) while averaging over 500 samples to reduce noise.

### B. Measurement Locations and Procedure

All measurements were performed on the fourth floor of Durham Hall, a modern engineering building, on the campus of Virginia Tech. The Tx and Rx antennas were placed in a variety of rich multipath environments such as hallways, offices and a dense laboratory environment.

We have chosen three different antenna heights for the measurements: 108.5 cm, 26.5 cm, and 7.5 cm. Furthermore, these will be referred as above ground (AG), middle ground

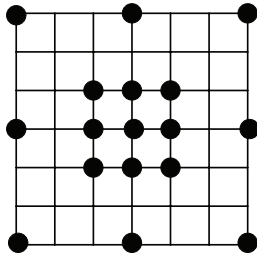


Fig. 1. Grid Layout

(MG), and near ground (NG) respectively. The height of the Tx and Rx antennas have been kept the same to keep the analysis simple. The receiving antenna was placed at 17 positions on a 90 cm 7x7 square grid, as shown in Figure 1. The grid is placed at various locations denoted by  $1, 2 \dots m \dots N$ . Additionally, we took some measurements at three locations with 13 different heights and fixed antenna separation. The results from the later measurements will be used to explain the effect of antenna height on the SSC in particular.

### III. MEASUREMENT ANALYSIS

The data analysis can be divided into four sections: path loss, shadowing, small scale fading, and small-scale time statistics. The first three sections examine the statistics of the entire received power delay profile (PDP). The last section investigates the time distribution of the energy throughout the received channel impulse response (CIR) by calculating the delay statistics such as RMS delay spread, mean excess delay, and the number of discrete multipath components.

#### A. Path Loss

Path loss is often used for link budget calculations and determining feasible transceiver ranges. In the simple single slope path loss model, at a Tx/Rx separation of  $d$ , the path loss is modeled as [11]:

$$PL(d) = PL_0 + n 10 \log_{10} \left( \frac{d_0}{d} \right) + X_0 \quad (1)$$

where  $PL_0$  is the path loss at a reference measurement  $d_0$ , and  $X_0$  represents “shadowing”. In our analysis, a 1 m Tx/Rx separation measurement was used as the reference. The path loss is represented by a single exponent  $n$ . The path loss exponent can be estimated from statistical inference of the measured data [12]. It is worth mentioning that a few past results [6], [13], [14] indicate the presence of a two slope path loss model in indoor cases. In this model, after a break point distance, the path loss exponent changes significantly from the previous value. But, these models do not fit into our measurement data. Hence we restrict ourselves to single slope path loss model only.

#### B. Shadowing

In (1),  $X_0$  is a log normal random variable with zero mean and standard deviation  $\sigma_s$ . This represents “shadowing” which is defined as the variation of the actual received power about

the average received power at distance  $d$ . Here, shadowing is calculated directly from the variation of  $PL(d)$  about the expected path loss.

#### C. Small Scale Fading

Fading is the variation of the received power due to the way that multipath components combine at the receiver. It is generally detrimental to the performance of narrowband systems. UWB systems are less affected by fading because the large bandwidth allows the multipath components to be resolved and collected using a Rake receiver. This leads to improved performance. Even though for UWB the effect is less severe, fading still exists. Therefore, one should not neglect the local power variation in the case of UWB. In our analysis, local fading is assumed to adopt a log normal distribution similar to that of shadowing. The average power  $\bar{P}_r^{(m)}$  over the  $m^{th}$  grid was calculated as:

$$\bar{P}_r^{(m)}(\bar{d}) = \frac{1}{|S|} \sum_{(i,j) \in S} \left[ \frac{1}{T} \int_0^T |r_{i,j}^{(m)}(t)|^2 dt \right] \quad (2)$$

where  $T = 50$  ns is the observation time,  $r_{i,j}^{(m)}(t)$  is the received time-varying signal at the point  $i, j$  in  $m^{th}$  grid.  $S$  is a set containing all 17  $i, j$  pairs on the grid.  $\bar{d}$  is the average distance between Tx and Rx which in our case is the distance between Tx and center of grid. The deviation of the received power  $P_{i,j}^{(m)}$  at grid point  $i, j$  from  $\bar{P}_r^{(m)}$  is given by:

$$\zeta_{i,j}^{(m)} = \frac{P_{i,j}^{(m)}}{\bar{P}_r^{(m)}} \left( \frac{\hat{d}_{i,j}^{(m)}}{\bar{d}^{(m)}} \right)^{n^{(m)}} \quad (3)$$

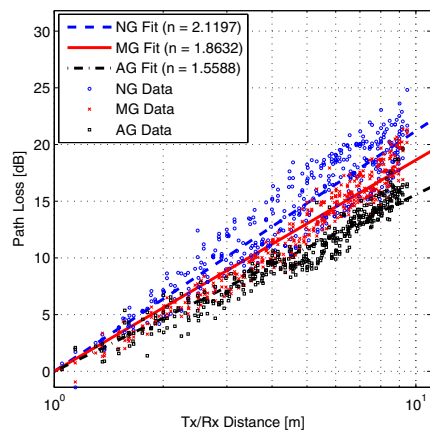
where  $\hat{d}_{i,j}^{(m)}$  is the distance between the Tx and the grid point  $i, j$ , and  $n^{(m)}$  is the path loss exponent. One can think (3) to be the difference between the received power and the expected power at the point  $i, j$  of the grid. Assuming a zero mean log-normal distribution, the fading variance is  $\sigma_f^2 = E \left\{ [10 \log_{10}(\zeta)]^2 \right\}$  over all  $i, j$  and  $m$ .

Furthermore, fading can be also modeled with a Rician (for LOS only) or Nakagami distribution. To estimate the Nakagami parameter  $s$ , we use the estimation technique described in [15]. Furthermore, for  $s > 1$ , the Rician factor  $K$  can be calculated from  $s$  using [16]:

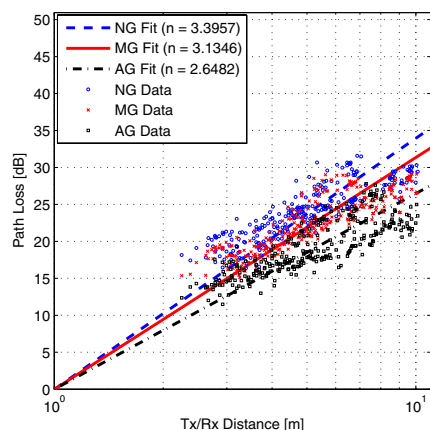
$$s = \frac{(K+1)^2}{2(K+1)} \quad (4)$$

#### D. Small Scale Time Characteristics

Small scale models quantify the energy distribution throughout a fixed observation time window. It often assumes a discrete number of received paths. For analysis purposes, we resolve the received PDPs into discrete time paths, called the channel impulse response (CIR). Since measurements were observed in the time domain, the CLEAN algorithm was used to deconvolve the received signal and the reference pulse to obtain the CIR. For more details on the CLEAN algorithm, the



(a) LOS



(b) NLOS

Fig. 2. Relative path loss for given antenna heights in LOS and NLOS scenarios

interested reader is referred to [17]. We adopt a finite stationary linear tap delay line model [11] for CIR which is given as:

$$h(t) = \sum_k \beta_k \delta(\tau - \tau_k) \quad (5)$$

where  $\beta_k$  and  $\tau_k$  are the real amplitude and excess delays, respectively, of the  $k^{th}$  multipath component. The maximum value for  $\tau_k$  can be equal to observation time  $T = 50$  ns. The multipath in the channel can be characterized by the first moment and the square root of the second central moment, which are also known as the mean excess delay and the RMS delay spread, respectively. Other important small scale statistics include the average number of discrete paths ( $N_p$ ) for the measured data (all nonzero elements of the CIR).

Using the above small scale statistics, one can develop a channel model for the given scenario. For small scale channel modeling, this paper uses the modified Saleh-Valenzuela (SV) model [18]. SV model assumes clustering of rays. Within the clusters, parameters  $1/\lambda$  and  $\gamma$  describe the mean ray inter-arrival rate and exponential amplitude decay respectively of

TABLE I  
LARGE CHANNEL STATISTICS

	Above Ground		Middle Ground		Near Ground	
	LOS	NLOS	LOS	NLOS	LOS	NLOS
$n$	1.56	2.65	1.86	3.13	2.12	3.40
$\sigma_s$ (dB)	1.03	2.41	1.25	2.56	1.88	2.76

TABLE II  
AVERAGE SMALL SCALE CHANNEL STATISTICS

	Above Ground		Middle Ground		Near Ground	
	LOS	NLOS	LOS	NLOS	LOS	NLOS
$\sigma_f$ (dB)	0.79	1.03	0.68	1.06	0.84	1.17
$\tau_{rms}$ (ns)	6.69	15.50	6.21	17.80	10.49	18.36
$\bar{\tau}$ (ns)	7.58	10.03	7.00	10.79	8.39	10.17
$N_p$	121	110	75	140	206	128
$K$ (dB)	15.9	-	16.1	-	14.6	-
$s$	20.27	16.99	21.20	16.76	15.20	16.38

a Poisson process. The clusters themselves are also Poisson processes with respective parameters  $1/\Lambda$  and  $\Gamma$ . Finally, the parameter  $\sigma$  is the standard deviation of the log-normal distributed path powers which combines the log-normal variations of the clusters and rays.

#### IV. MEASUREMENT RESULTS & DISCUSSION

##### A. Path loss

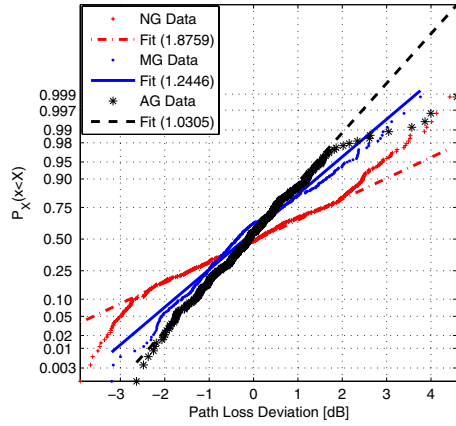
The results from the path loss analysis are shown in Figure 2 (a) and (b) for LOS and NLOS case respectively. It can be seen that for both cases NG has the highest path loss exponent (2.1 and 3.4) and AG has the lowest path loss exponent (1.6 and 2.6). MG path loss exponents are in the middle (1.7 and 3.1). Therefore, Figure 2 indicates that path loss increases while decreasing the antenna height. This result is consistent with the results presented in [3], [8] although the difference between path loss for given heights is less here. This is because in the current paper, the measurement sites chosen are narrower in dimension as compared to previous papers. Specifically, [8] reported an AG path loss exponent of 1.27, and 1.85 for LOS and NLOS respectively and a NG path loss of 2.50 and 3.50 for LOS and NLOS respectively. The results in [8] show a noticeably lower AG NLOS path loss, which can be attributed to the specific environments examined.

##### B. Shadowing

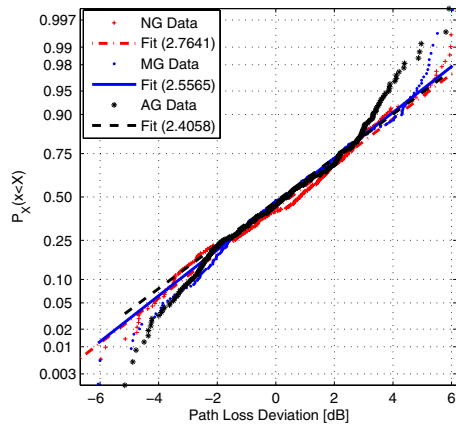
Figure 3 shows that shadowing increases, (1.03, 1.24, and 1.9 in LOS case, and 2.41, 2.56, 2.76 in NLOS case, for AG, MG, and NG respectively) while lowering the antenna. This result is also consistent to the results given in [8]. Here it is extended to three heights and solidifies our previous observations. The statistics for path loss and shadowing are summarized in Table I.

##### C. Small Scale Characteristics (SSC)

The SSCs (namely fading, RMS delay, mean delay and number of paths) are presented in Table II. In LOS scenario, all of the SSC show an interesting behavior, i.e., the MG case



(a) LOS



(b) NLOS

Fig. 3. Cumulative distributions of shadowing variations about the mean path loss model and their fits to log-normal distributions

characteristics are either the highest or the lowest. The MG case has the lowest values ( $\tau_{\text{rms}} = 6.21$  and  $17.80$  ns, and  $\bar{\tau} = 7.00$  and  $10.79$  ns for the LOS and NLOS case respectively) and NG case has the highest ( $\tau_{\text{rms}} = 10.49$  and  $18.36$  ns, and  $\bar{\tau} = 8.39$  and  $10.17$  ns for the LOS and NLOS case respectively). On the other hand, the Rician factor  $K$  is highest (16.1) for the MG case and lowest for the NG case (14.6).

In another set of measurements, the RMS delay values for 13 different antenna heights are calculated and averaged for three different locations. The results are presented in Figure 4. In Figure 5, the dominant CIR component is shown for the corresponding antenna heights. Table III presents the estimated S-V parameters.

The behavior of the characteristics in Table II can be described with the help of Figures 4 and 5. As shown in Figure 4, RMS delay is highest for very low antenna heights and initially decreases on increasing antenna height. But after some height, the increase in antenna height leads to an increase in RMS delay again and then to fluctuations. This behavior is due to the

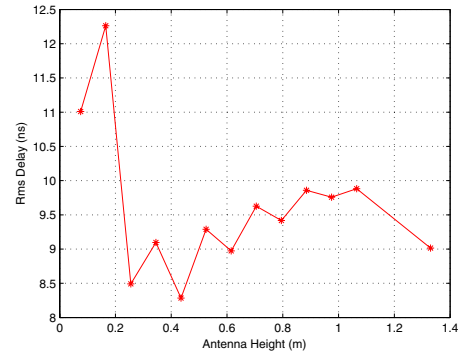


Fig. 4. RMS delay for different antenna heights

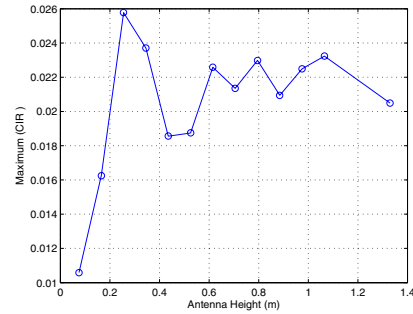


Fig. 5. Variation of direct LOS component for different heights

assumption that the receiver has a fixed dynamic range. When this condition applies, only those multipath are collected at the receiver whose power levels lie in the range  $\{P_d, P_d - T_H\}$ . Where  $P_d$  is the power of the dominant multipath component and  $T_H$  is a threshold limit, both in dB.  $T_H$  is equal to the assumed dynamic range of the receiver. In our results  $T_H$  it was assumed to be 20 dB. In other words, all multipath components that are 20 dB below the dominant path are ignored. Therefore, the strength of the dominant path (possibly LOS) affects the number of resolved multipath components. A smaller number of multipath components generally results to a decreased RMS delay spread.

Furthermore, it is worth indicating that Figure 5 appears to be inversely related to Figure 4. In Figure 5, the dominant CIR component is higher for middle antenna heights as compared to very low or high antenna heights. This observation, paired with the discussion about the receiver's dynamic range, explains the fluctuations of the RMS delay. However, this begs the question as to why the dominant CIR component exhibits this behavior with respect to height. This can be explained using a 2-ray ground model [11]. Even though a 2-ray ground model is a highly simplified model for the indoor UWB channel, it provides useful insight into the reasons behind the obtained results. This model becomes more applicable when the antennas are near the ground since the second strongest component is likely to be a ground-reflected ray. Also, in

TABLE III  
SALEH-VALENZUELA CHANNEL MODEL PARAMETERS

	Above Ground		Middle Ground		Near Ground	
	LOS	NLOS	LOS	NLOS	LOS	NLOS
$1/\Lambda(ns)$	11	11.25	13.75	9.48	11	5
$1/\lambda(ns)$	0.1	0.58	0.1	0.58	0.1	0.1
$\Gamma(ns)$	11.5	24.95	11.88	23.5	16	23.5
$\gamma(ns)$	2.63	5.08	2.44	6.00	5.25	4.50
$\sigma(dB)$	6.05	3.17	7.17	3.08	6.05	9.03

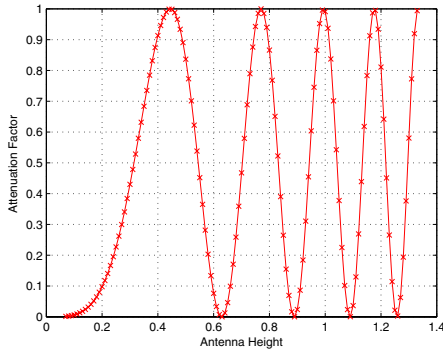


Fig. 6. Variation of 2-ray ground model attenuation factor with respect to antenna height (in meters)

the near-ground model, the ground reflected ray may not be resolvable, unlike in above-ground propagation. According to this model, the received signal strength  $P_r(d)$  can be given as:

$$P_r(d) = 4P_{dir} \sin^2 \left( \frac{2\pi h_t h_r}{\lambda d} \right) \quad (6)$$

where  $P_{dir}$  is the power of the direct ray at receiver,  $d$  is the distance between Tx and Rx and  $h_t$ ,  $h_r$  are the Tx, Rx heights respectively. Hence for a fixed value of  $d$ , the received energy depends on Tx/Rx antenna heights and wavelength  $\lambda$ .  $\lambda$  is calculated using the center of the 10 dB Bandwidth of the received UWB signal (1.55 GHz). The  $\sin^2(\cdot)$  component can be seen as an attenuation factor. The variation of attenuation factor with respect to antenna height is shown in Figure 6. As expected, this factor has an oscillatory behavior. For the heights taken in AG and NG case, we have a very high attenuation factor (around 0.01). But for MG case, it is around 0.3. This provides some insight into the behavior in Figure 5.

In NLOS conditions, RMS delay and fading decrease with an increase in antenna height which is again due to the strongest component decreasing with a decrease in height. It is important to note that the behavior of the RMS delay in the indoor scenario is different from outdoor scenarios where RMS delay increases with a decrease in antenna height. Therefore, in indoor cases, RMS delay and other SSC also depend heavily on the environment characteristics apart from antenna height. Our results support this intuition.

## V. CONCLUSION

This paper characterizes the indoor UWB channel for three different antenna heights. The large scale characteristics, i.e.,

path loss and shadowing, show behavior which is consistent with previous work, i.e. monotonically increasing attenuation with decreasing antenna height. However, the SSC show an interesting pattern that can be explained using a 2-ray ground model. It is shown that the SSC do not show a straight forward behavior with respect to antenna height. They also depend heavily on the environment. The knowledge of the behavior of the SSC will be helpful particularly in the receiver design for discussed applications.

## REFERENCES

- [1] C.-C. Chong, Y. Kim, and S.-S. Lee, "UWB indoor propagation channel measurements and data analysis in various types of high-rise apartments," in *IEEE 60th Vehicular Technology Conference*, vol. 1, September 2004, pp. 150–154.
- [2] N. R. Adam, V. Atluri, and V. P. Janeja, "Poster on secure agency interoperation for border control and homeland security applications," in *2nd Symposium on Intelligence and Security Informatics*, June 2004.
- [3] R. A. Foran, T. B. Welch, and M. J. Walker, "Very near ground radio frequency propagation measurements and analysis for military applications," in *IEEE Military Communications Conference Proceedings*, vol. 1, 1999, pp. 336–340.
- [4] Q. Li and W. S. Wong, "Measurement and analysis of the indoor uwb channel," in *IEEE 58th Vehicular Technology Conference*, vol. 1, Oct. 2003, pp. 1–5.
- [5] G. Durisi and G. Romano, "Simulation analysis and performance evaluation of an UWB system in indoor multipath channel," in *IEEE Conference on Ultra Wideband Systems and Technologies*, May 2002, pp. 255–258.
- [6] D. Cassioli, M. Z. Win, and A. F. Molisch, "The ultra-wide bandwidth indoor channel: from statistical model to simulations," *IEEE Journal on Selected Areas in Communications*, vol. 20, no. 6, pp. 1247–1257, Aug 2002.
- [7] J. R. Foerster, "The effects of multipath interference on the performance of UWB systems in an indoor wireless channel," in *IEEE 53rd Vehicular Technology Conference*, vol. 2, 2001, pp. 1176–1180.
- [8] A. Hugine, H. Volos, J. Gaeddert, and R. M. Buehrer, "Measurement and characterization of the near-ground indoor ultra wideband channel," in *IEEE Wireless Communications and Networking Conference*, vol. 2, 2006, pp. 1062–1067.
- [9] K. Sohrabi, B. Manriquez, and G. J. Pottie, "Near ground wideband channel measurement in 800-1000 MHz," in *IEEE 49th Vehicular Technology Conference*, vol. 1, Jul 1999, pp. 571–574.
- [10] G. G. Joshi, C. B. Dietrich, C. R. Anderson, W. G. Newhall, W. A. Davis, J. Isaacs, and G. Barnett, "Near-ground channel measurements over line-of-sight and forested paths," *IEE Proceedings of Microwaves, Antennas and Propagation*, pp. 589–596, Dec. 2005.
- [11] T. S. Rappaport, *Wireless Communications : Principles and Practice*, 2nd ed. New Jersey: Prentice Hall, 2002.
- [12] S. S. Ghassemzadeh, L. J. Greenstein, A. Kavcic, T. Sveinsson, and V. Tarokh, "UWB indoor path loss model for residential and commercial buildings," in *IEEE 58th Vehicular Technology Conference*, vol. 5, Oct. 2003, pp. 3115–3119.
- [13] B. Alavi, N. Alsindi, and K. Pahlavan, "UWB Channel Measurements for Accurate Indoor Localization," in *Military Communications Conference*, Oct. 2006, pp. 1–7.
- [14] M. Dohler, B. Allen, A. Armogida, S. McGregor, M. Ghavami, and H. Aghvami, "A new twist on UWB pathloss modelling," in *IEEE 59th Vehicular Technology Conference*, vol. 1, May 2004, pp. 199–203.
- [15] J. Gaeddert and A. Annamalai, "Further results on nakagami-m parameter estimation," *IEEE Communications Letters*, vol. 9, January 2005.
- [16] L.-C. Wang and C.-T. Lea, "Co-channel interference analysis of shadowed rician channels," *IEEE Communications Letters*, vol. 2, no. 2, March 1998.
- [17] J. H. Reed, *An Introduction to Ultra Wideband Communications Systems*. Crawfordsville, Indiana: Prentice Hall, 2005.
- [18] A. Molisch, Foerster, and M. J.R. Pendergrass, "A Statistical Model for Indoor Multipath Propagation," *IEEE Wireless Communications*, vol. 10, no. 6, pp. 14–21, Dec 2003.